nature neuroscience

Synapse-specific plasticity and compartmentalized signaling in cerebellar stellate cells

Gilberto J Soler-Llavina[1] & Bernardo L Sabatini[1]

Here we demonstrate that cerebellar stellate cells diffusionally isolate synaptically evoked signals in dendrites and are capable of input-specific synaptic plasticity. Sustained activity of parallel fibers induces a form of long-term depression that requires opening of calcium (Ca^{2+})-permeable AMPA-type glutamate receptors (CP-AMPARs) and signaling through class 1 metabotropic glutamate receptors (mGluR1) and CB1 receptors. This depression is induced by postsynaptic increases in Ca^{2+} concentration ([Ca^{2+}]) and is limited to activated synapses. To understand how synapse-specific plasticity is induced by diffusible second messengers in aspiny dendrites, we examined diffusion of Ca^{2+} and small molecules within stellate cell dendrites. Activation of a single parallel fiber opened CP-AMPARs, generating long-lived Ca^{2+} transients that were confined to submicron dendritic stretches. The diffusion of Ca^{2+} was severely retarded due to interactions with parvalbumin and a general restriction of small molecule mobility. Thus stellate cell dendrites spatially restrict signaling cascades that lead from CP-AMPAR activation to endocannabinoid production and trigger the selective regulation of active synapses.

Many forms of synaptic plasticity are induced by the accumulation of diffusible second messengers. Therefore, the independent regulation of individual synapses requires dendritic specializations that biochemically isolate each synapse from its neighbors. In principal neurons, such as cerebellar Purkinje cells, hippocampal and cortical pyramidal cells and striatal medium spiny neurons, the sequestration of glutamatergic synapses onto heads of dendritic spines is thought to provide the diffusional isolation necessary for independent regulation of each synapse (reviewed in ref. 1).

In contrast, most GABAergic interneurons lack dendritic spines and receive excitatory input directly onto the dendritic shaft[2,3]. Furthermore, plasticity of glutamatergic synapses onto interneurons often occurs heterosynaptically, such that synapses that did not experience the induction protocol are also modified[4,5]. Nevertheless, the spatial confinement of synaptically evoked signals has been described in dendrites of several classes of interneurons. In rat hippocampal CA1 and cortical layer 2/3 bitufted interneurons, synaptically evoked Ca^{2+} signals spread over $\sim$10 μm of dendrite[6–8], a length that is likely to encompass multiple synapses. In contrast, in mouse cortical fast-spiking interneurons, synaptically evoked Ca^{2+} signals are restricted to $\sim$1 μm compartments near active synapses[9]. It is unknown if this difference in the spread of Ca^{2+} signals is functionally significant—that is, if it determines or correlates with the spatial extent of activation of downstream Ca^{2+}-dependent processes.

Stellate cells of the cerebellum have been extensively studied, and previous findings make it particularly interesting to examine dendritic compartmentalization in these cells. Stellate cells are aspiny interneurons that receive glutamatergic inputs from a small set of granule cells via parallel fibers and whose outputs regulate Purkinje cell firing via GABAergic synapses[2,10]. Postsynaptically induced, Ca^{2+}-dependent forms of long-term plasticity have been described at synapses between parallel fibers and stellate cells; however, input specificity remains unexplored[11,12]. Furthermore, stellate cells express Ca^{2+}-permeable ionotropic receptors at the synapse, whose activation is predicted to trigger focal Ca^{2+} increases in the dendrite. Also, stellate cells express the Ca^{2+}-binding protein parvalbumin, which may slow the diffusion of Ca^{2+} by its sequestration[13].

Here we describe a new form of long-term depression at parallel fiber–to–stellate cell synapses, termed stellate cell long-term depression (SCLTD), which shows input specificity and requires the opening of Ca^{2+}-permeable AMPA-type glutamate receptors (CP-AMPARs), postsynaptic Ca^{2+} accumulation and the activation of mGluR1. SCLTD differs from previously described forms of LTD at the parallel fiber–to–stellate cell synapse because its expression requires signaling through CB1 receptors and is independent of switching of AMPAR subtypes. We show that the Ca^{2+} signals responsible for SCLTD induction are highly compartmentalized within stellate cell dendrites. The accumulation of Ca^{2+} entering through CP-AMPARs is confined to an $\sim$1-μm segment of dendrite surrounding individual active synapses. This compartmentalization results from a parvalbumin-dependent restriction of Ca^{2+} diffusion as well as from a general retardation of small molecule mobility within the dendrite. In summary, our results reveal that stellate cells possess multiple mechanisms that functionally compartmentalize dendrites and allow active synapses to be selectively depressed by signaling cascades that rely on multiple diffusible factors.

[1]Department of Neurobiology, Harvard Medical School, 220 Longwood Avenue, Boston, Massachusetts 02115, USA. Correspondence should be addressed to B.L.S. (bsabatini@hms.harvard.edu).

Received 21 March; accepted 17 April; published online 7 May 2006; doi:10.1038/nn1698

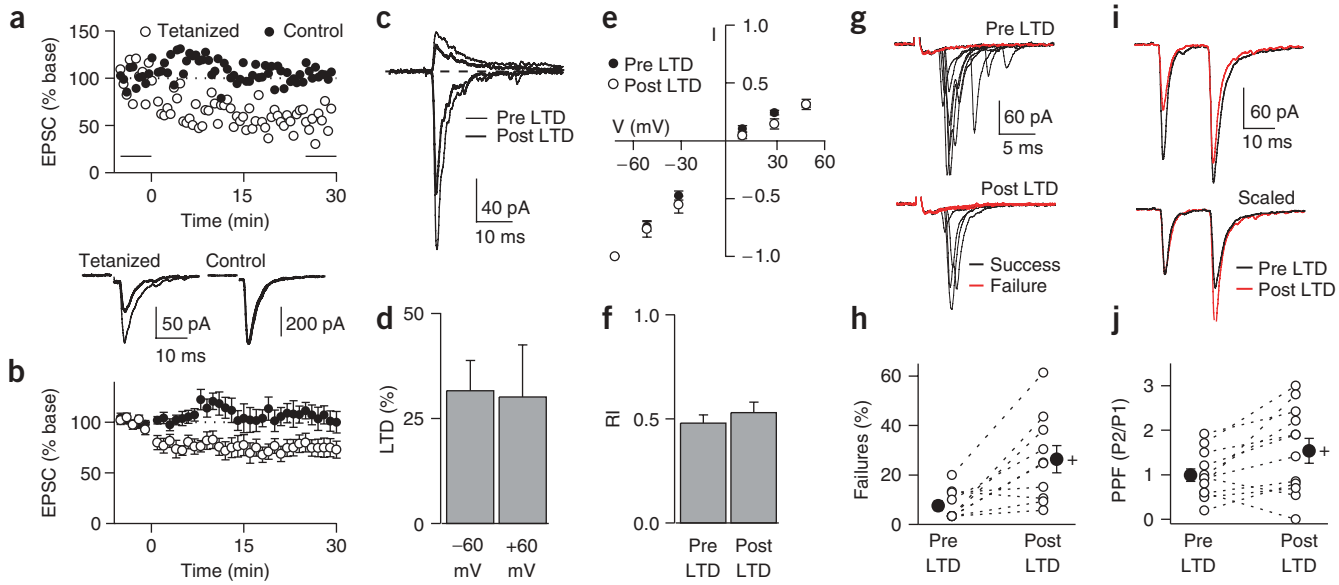

Figure 1 Trains of stimuli induce input-specific LTD at the parallel fiber–to–stellate cell synapse. (**a**) Top, time course of an experiment showing the effect of trains of synaptic activity on the EPSC in a tetanized pathway and a control pathway. Bottom, average EPSC in each pathway measured during the baseline period (thin line) and 25–30 min after LTD induction (thick line). (**b**) Pooled data from 14 cells. (**c**) EPSCs (average of 30 trials) recorded at holding potentials of –60 mV and 60 mV before and after LTD induction. (**d**) Percentage LTD of EPSCs at –60 mV and +60 mV. (**e**) Normalized *I-V* relationships before and after LTD induction. (**f**) The rectification index of the EPSC measured before and after LTD induction. Data in **c**–**f** are from the same cells ($n = 6$). (**g**) EPSCs (10 consecutive trials) measured before and after LTD induction in an experiment that showed synaptic failures in the baseline period. (**h**) The EPSC failure rates for single experiments (open circles) and the mean failure rates (filled circles, $n = 10$) before and after LTD induction. (**i**) Paired EPSCs (average of 15 trials) measured before and after LTD induction. The scaled version of these EPSCs is shown below. (**j**) PPF for individual experiments (open circles) and mean PPF (filled circles, $n = 12$) measured during the baseline period and after LTD induction. $+P < 0.02$.

RESULTS

LTD at parallel fiber to stellate cell synapses

Stellate cells in acute cerebellar slices from juvenile rats were placed under whole-cell voltage clamp, and the responses of two independent sets of parallel fiber inputs were monitored. Repetitive stimulation (4×25 stimuli at 30 Hz, delivered at 0.33 Hz) induced a decrease in the amplitude of the excitatory postsynaptic current (EPSC) in the tetanized pathway but had no effect on the control, untetanized pathway (**Fig. 1a**). We refer to the synaptic depression induced by this protocol as SCLTD and report its magnitude as the percentage reduction in EPSC amplitude measured 25–30 min after the tetanus. The magnitude of SCLTD was 27 ± 6.8% and –3.4 ± 11.8% in the tetanized and control pathways, respectively (**Fig. 1b**).

Prolonged parallel fiber stimulation induces a switch in the AMPAR composition at parallel fiber–to–stellate cell synapses, such that Ca^{2+}-impermeable AMPARs (CI-AMPAR) replace CP-AMPARs (ref. 11). In the presence of intracellular polyamines, CP-AMPARs are inwardly rectifiying whereas current flow through CI-AMPAR remains linear[14–16]. Thus, if SCLTD involves the replacement of CP-AMPARs with CI-AMPARs, its induction should linearize the current-voltage relationship and depress current flow at negative potentials more than at positive potentials. We found that the magnitude of depression induced in the presence of intracellular spermine was identical for synaptic currents monitored at –60 mV and +60 mV, and was not different from that observed in spermine-free recordings (**Fig. 1c,d**). Furthermore, the rectification index (RI) of EPSCs did not change after the induction of SCLTD ($RI_{preLTD} = 0.48 \pm 0.05$; $RI_{postLTD} = 0.53 \pm 0.05$) (**Fig. 1e,f**).

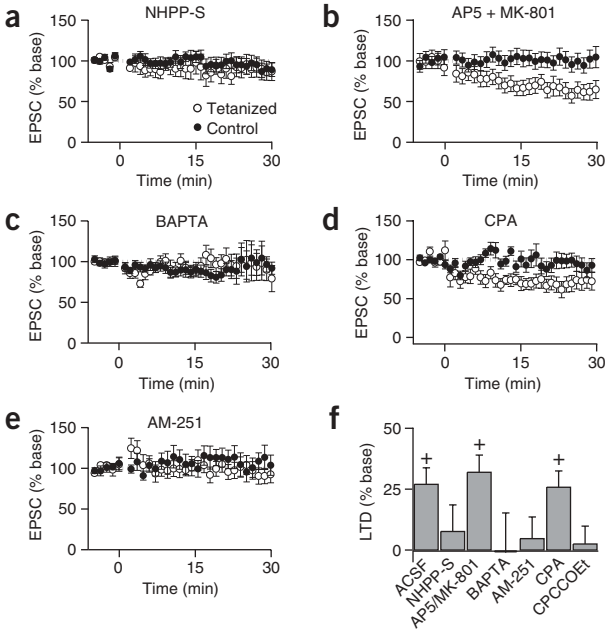

Figure 2 SCLTD requires AMPAR-mediated postsynaptic Ca^{2+} increases and CB1 receptor activation. (**a**,**b**) Summary of EPSC amplitudes in the tetanized and control pathways in the presence of NHPP-spermine ($n = 14$) or NMDAR antagonists (pooled data from $n = 10$ with AP5 alone and $n = 10$ with AP5 + MK-801), respectively. (**c**) Summary of EPSC amplitudes as in **a** for cells loaded through the patch pipette with the Ca^{2+} chelator BAPTA ($n = 13$). (**d**,**e**) Summary of EPSC amplitudes in the tetanized and control pathways measured in the presence of CPA ($n = 8$) and AM-251 ($n = 8$), respectively. (**f**) Magnitude of LTD observed in each pharmacological condition. $+P < 0.05$.

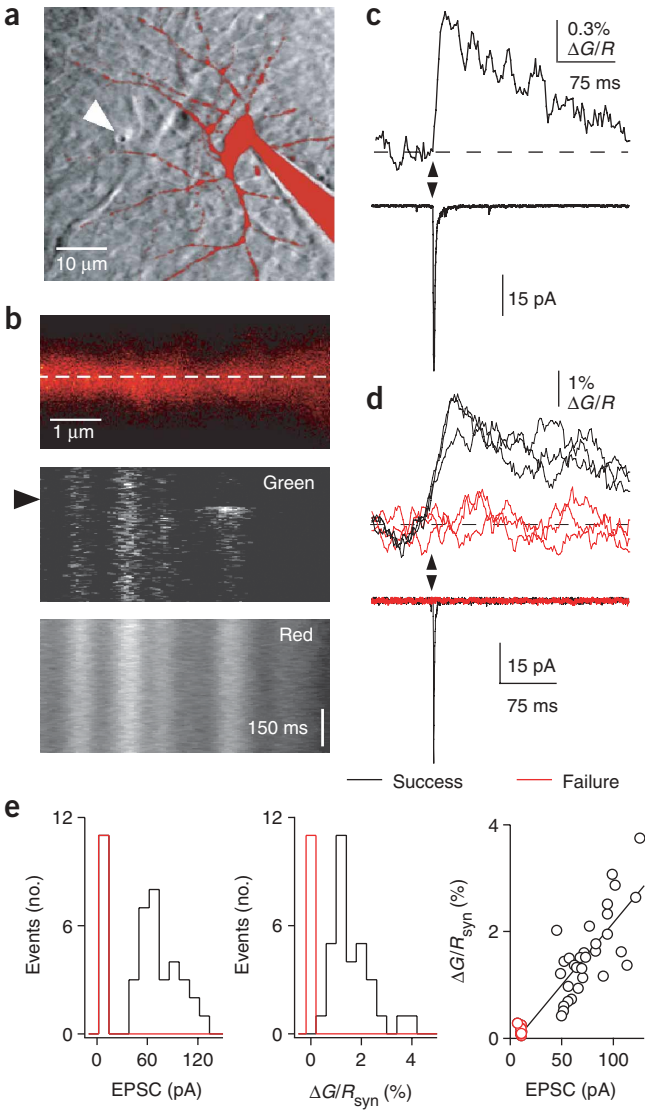

Figure 3 Synaptically evoked Ca^{2+} transients in dendrites of cerebellar stellate cells. (**a**) Image of a stellate cell (Alexa-594 fluorescence) overlaid on a laser-scanning DIC image of the slice. Arrowhead, position of the stimulating electrode in the molecular layer. (**b**) Enlarged image of a stellate cell dendrite indicating the orientation of the line scan (dashed line) used for $\Delta[Ca^{2+}]_{syn}$ measurements. Green (Fluo-5F) and red (Alexa-594) fluorescence, collected in line scan mode during electrical stimulation of parallel fibers. Arrowhead, time of stimulation. Green and red images are averages of 42 consecutive trials. (**c**) Top, quantification of the fluorescence transient shown in **b**. Bottom, average EPSC. (**d**) Representative fluorescence transients (top) and EPSCs (bottom) showing successes and failures of synaptic transmission. (**e**) Histograms of EPSC (left) and $\Delta G/R_{syn}$ (middle) amplitudes with data from failure trials shown in red. $\Delta G/R_{syn}$ plotted against EPSC amplitude (right) for the 42 trials. Solid line is a linear regression ($r^2 = 0.87$). All data in panels **b**–**e** are from the same experiment.

Three lines of evidence indicate that SCLTD is a presynaptically expressed form of LTD mediated by changes in the probability of glutamate release. First, SCLTD induction increased the coefficient of variation of EPSC amplitude (CV_{EPSC}) from 38 ± 2.2% to 53 ± 4.5% ($P < 0.01$, $n = 34$). CV_{EPSC} in the control pathway was unaffected (baseline = 32 ± 1.7%; post-tetanus = 38 ± 2.9%). Second, among the experiments performed in conditions that allow SCLTD induction, ten showed failures in the tetanized pathway during the baseline period, and the failure rate increased in these cells after SCLTD induction from 7.6 ± 1.9% to 26.4 ± 5.5 % (**Fig. 1g**,**h** and **Supplementary Fig. 1** online). Last, paired-pulse facilitation (PPF) measured at a 15-ms interstimulus interval increased after SCLTD induction from 1.99 ± 0.15 to 2.55 ± 0.27 (**Fig. 1i**,**j**).

SCLTD requires $[Ca^{2+}]$ increases and CB1R activation

The inward rectification of synaptic currents in the basal state indicates that CP-AMPARs are present in the synapse[11]. Stellate cells also express NMDA-type glutamate receptors (NMDARs) that can be activated by strong parallel fiber stimulation[17]. We examined whether Ca^{2+} influx through these receptors and the subsequent Ca^{2+} buildup in the dendrite are required for SCLTD. N-(4-hydroxyphenylpropanyl) spermine (NHPP-S) (10–50 µM), a use-dependent blocker of CP-AMPARs (ref. 18), prevented the induction of SCLTD (percent LTD = 7.62 ± 10.9) (**Fig. 2a**). In contrast, the NMDAR antagonist D-2-amino-5-phosphonopentanoate (AP5, 20 µM) or a combination of AP5 and MK-801 (100 µM and 50 µM) had no effect on SCLTD induction. Results from both pharmacological conditions were similar and were pooled (percent LTD = 31.9 ± 7.1) (**Fig. 2b**). Inclusion of the rapid Ca^{2+} chelator BAPTA (20 mM) in the intracellular solution prevented SCLTD (percent LTD = –1.1 ± 16) (**Fig. 2c**), indicating that it requires increases in postsynaptic $[Ca^{2+}]$. As the inclusion of BAPTA in the single voltage-clamped neuron prevented depression, it follows that SCLTD must be induced cell autonomously. Finally, bath application of cyclopiazonic acid (CPA, 50 µM), which blocks the smooth endoplasmic reticulum Ca^{2+}-ATPase and depletes intracellular Ca^{2+} stores (**Supplementary Fig. 2** online), did not prevent SCLTD, indicating that Ca^{2+} release from internal stores is not necessary for its induction (**Fig. 2d**).

Parallel fibers express the endocannabinoid receptor CB1 (CB1R)[19], and its activation mediates short-term plasticity at synapses onto Purkinje cells[20,21] and stellate cells[22]. Production of endocannabinoids in Purkinje cells is triggered by AMPAR activation in a Ca^{2+}-dependent manner[20,23,24] and is required for LTD induction[25]. Similarly, bath application of the CB1R antagonist AM-251 prevented the induction of SCLTD (percent LTD = 4.7 ± 8.9) (**Fig. 2e**). SCLTD induction was also prevented by the mGluR1 antagonist CPCCOEt (**Fig. 2f** and **Supplementary Fig. 3** online; percent LTD = 2.1 ± 7.3), consistent with previous findings demonstrating a facilitatory role of mGluR1 activation in endocannabinoid-mediated synaptic depression at the parallel fiber–to–Purkinke cell synapse[23].

Synaptically evoked Ca^{2+} transients in stellate cells

The above data indicate that stellate cells can selectively regulate active inputs and predict that stellate cell dendrites spatially confine the signaling cascades that underlie SCLTD. Thus we expect that synaptically evoked Ca^{2+} accumulations ($\Delta[Ca]_{syn}$) are confined to small dendritic stretches near active synapses. To test this prediction, we examined $\Delta[Ca]_{syn}$ in dendrites of voltage-clamped stellate cells using two-photon laser scanning microscopy (2PLSM). Stellate cells were loaded with a red-fluorescing morphological marker (20 µM, Alexa Fluor-594) and a green-fluorescing, low-affinity Ca^{2+} indicator (300 µM, Fluo-5F) (**Fig. 3a**). To monitor $\Delta[Ca]_{syn}$, green and red fluorescence were collected in a line oriented along a dendrite during the extracellular activation of parallel fibers (**Fig. 3b**) and quantified as increases in green fluorescence normalized to red fluorescence ($\Delta G/R_{syn}$)[26].

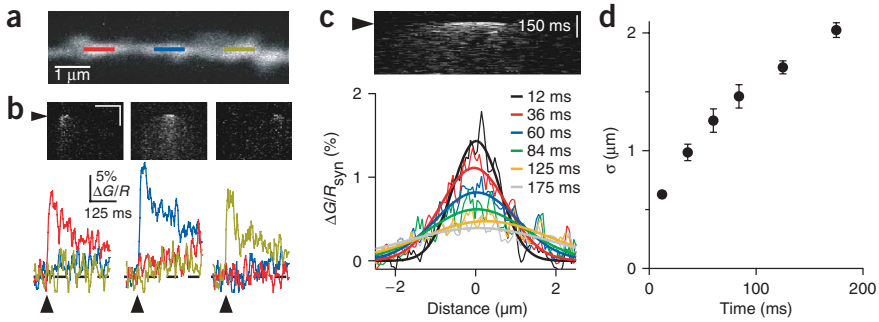

Figure 4 $\Delta[Ca^{2+}]_{syn}$ is restricted to submicron dendritic regions. (**a**) Image of a stellate cell dendrite with three regions that showed independent, synaptically evoked Ca^{2+} transients. (**b**) Green fluorescence collected in line scan mode (top) and quantification of the fluorescence transients (bottom) for three trials of synaptic stimulation from the dendrite shown in **a**. $\Delta G/R_{syn}$ is shown for each of the highlighted regions in **a** (red, blue, green lines). Scale bars, 2 µm and 150 ms. (**c**) Top, green fluorescence collected in line scans (average of 40 consecutive trials) during synaptic stimulation (arrowhead) in a dendrite of a stellate cell loaded with Fluo-5F. Bottom, profiles of $\Delta G/R_{syn}$ along the dendrite (noisy, thin traces) measured at various times after stimulation. Smooth lines are Gaussian fits. (**d**) Standard deviations of Gaussian fits to the dendritic fluorescence profiles (σ) plotted as a function of time ($n = 13$). Black arrowhead, time of stimulation.

EPSCs of similar amplitude (–65.4 ± 4.4 pA; $n = 40$) to spontaneous miniature EPSCs (refs. 22,27) increased green fluorescence within the dendrite near the stimulating electrode, consistent with an increase in $[Ca^{2+}]$ at active synapses (**Fig. 3b**). $\Delta G/R_{syn}$ had a rapid rising phase (8–12 ms) and a slow decay time constant ($\tau_{\Delta G/R} = 305.7 \pm 33$ ms), outlasting the EPSC by hundreds of milliseconds ($\tau_{EPSC} = 3.6 \pm 0.3$ ms; $n = 27$) (**Fig. 3c**). $\Delta G/R_{syn}$ appeared stochastically, and the presence and absence of fluorescence transients corresponded to successes and failures of the EPSC (**Fig. 3d**). Furthermore, in the success trials, the amplitudes of $\Delta G/R_{syn}$ and the EPSC covaried tightly (**Fig. 3e** and **Supplementary Fig. 4** online). On the basis of the stochastic, yet correlated, nature of $\Delta G/R_{syn}$ and the EPSC, we concluded that both signals are generated by current flow through a common set of receptors and that the site of evoked fluorescence changes in the dendrites indicates the position of the active synapse.

In a few experiments, multiple synaptic contacts were stimulated within the field of view (**Fig. 4a**). Each site responded independently to the extracellular stimulation (**Fig. 4b**), indicating that stellate cells possess mechanisms that prevent the spread of Ca^{2+} from active to inactive synapses. To measure the spread of synaptically evoked Ca^{2+} transients, we limited our analysis to experiments in which a single site was stimulated and $\Delta G/R_{syn}$ and EPSC amplitude covaried. The profiles of $\Delta G/R_{syn}$ as a function of the distance along the dendrite were well fit by Gaussian functions, consistent with spread by diffusion away from a focal source within a cylindrical (one-dimensional) structure (**Fig. 4c**)[9,28,29]. The standard deviation of the Gaussian fit (σ) gives the lateral spread of $\Delta[Ca]_{syn}$ within the dendrite. Immediately after stimulation, when the magnitude of the local Ca^{2+} transient is at its peak, $\Delta G/R_{syn}$ was localized to submicron compartments ($\sigma_{peak} = 0.63 \pm 0.04$ µm; $n = 13$) (**Fig. 4d**). The maximal spatial extent of $\Delta G/R_{syn}$ (σ_{max}) was reached at ~175 ms after stimulation (2.02 ± 0.13 µm). Beyond this time point, $\Delta G/R_{syn}$ was too small to be fit reliably.

Ca^{2+}-permeable AMPARs mediate synaptic Ca^{2+} influx

If $\Delta[Ca]_{syn}$ is responsible for SCLTD induction, it should result from the activation of CP-AMPARs but not NMDARs. The application of a cocktail containing the NMDAR antagonists AP5 (100 µM) and MK-801 (50 µM) had no effect on $\Delta G/R_{syn}$ (89.5 ± 5.8% of control) or the EPSC (104.1 ± 9.9% of control) (**Fig. 5a**). In addition, the spatial spread of $\Delta G/R_{syn}$ was the same in control conditions and in the presence of the NMDAR antagonists ($\sigma_{peak} = 0.55 \pm 0.05$ and $\sigma_{max} = 1.4 \pm 0.2$). Application of the AMPAR antagonist 2,3-dioxo-6-nitro-1,2,3,4-tetrahydrobenzo[f]quinoxaline-7-sulfonamide (NBQX, 10 µM) abolished $\Delta G/R_{syn}$ (3.7 ± 1.8% of control) and the EPSC (4.2 ± 0.6% of control), whereas NHPP-spermine (10–50 µM), an antagonist of CP-AMPARs, largely eliminated $\Delta G/R_{syn}$ (19.5 ± 6.0% of control) but blocked only a fraction of the EPSC (46.6 ± 9.0% of control) (**Fig. 5b,c**). This suggests that individual synapses contain a mixed population of CP-AMPARs and CI-AMPARs (refs. 8,11,30). Cyclothiazide

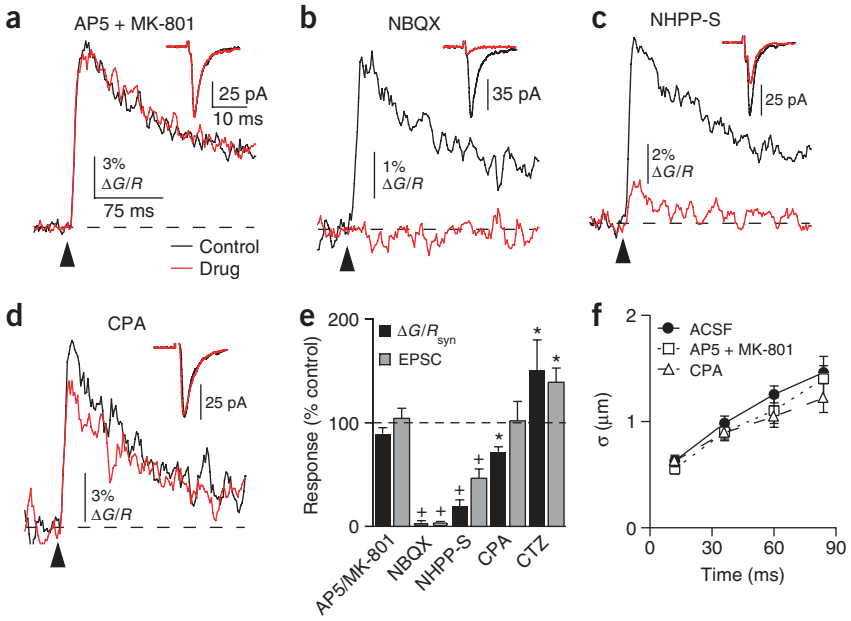

Figure 5 CP-AMPARs mediate $\Delta[Ca^{2+}]_{syn}$. (**a**) $\Delta G/R_{syn}$ in control conditions and after application of AP5 and MK-801 ($n = 7$). Insets, corresponding EPSCs. (**b–d**) As in **a**, after the application of NBQX ($n = 7$), NHPP-spermine ($n = 11$) and CPA ($n = 6$), respectively. (**e**) Summary of the effects of each manipulation on $\Delta G/R_{syn}$ and the EPSC (*$P < 0.05$; +$P < 0.01$). For experiments in CTZ, $n = 5$. (**f**) The spread of $\Delta G/R_{syn}$ along the dendrite as a function of time was unaffected by blockade of NMDARs (AP5 alone, or AP5 and MK-801, $n = 6$) or sarco-endoplasmic reticulum Ca^{2+}-ATPase (SERCA; CPA, $n = 6$). Data from **Figure 3d** is shown for comparison. Black arrowhead, time of stimulation.

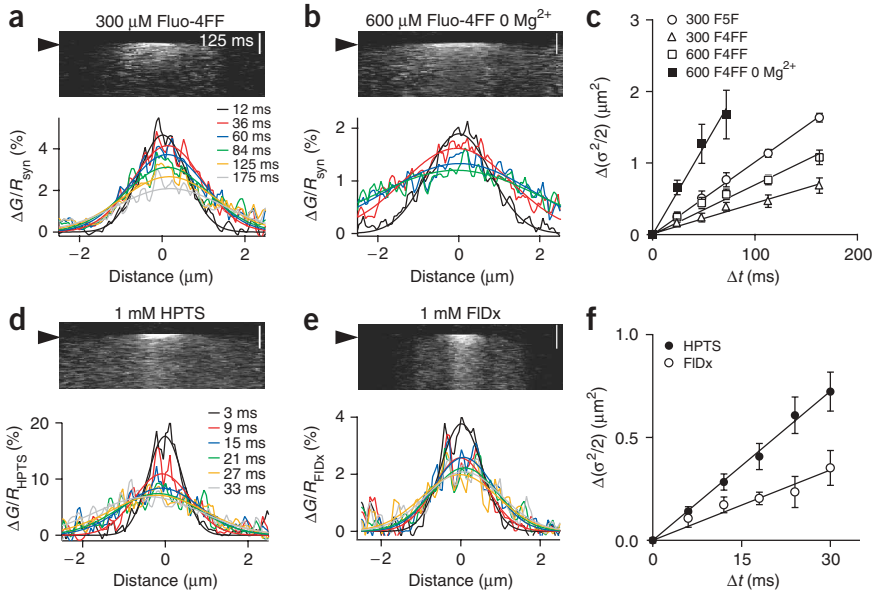

Figure 6 Mechanisms of Ca^{2+} compartmentalization in stellate cell dendrites. (**a**) Top, green fluorescence collected in line scans during synaptic stimulation in a dendrite loaded with 300 μM Fluo-4FF. Bottom, profile of $\Delta G/R_{syn}$ along the dendrite (noisy, thin traces) measured at various times after stimulation. (**b**) As in **a**, for cells loaded with a Mg^{2+}-free intracellular solution containing 600 μM Fluo-4FF. (**c**) $\Delta(\sigma^2/2)$ versus time after stimulation (Δt) measured in the presence of 300 μM Fluo-5F ($n = 13$), 300 μM Fluo-4FF ($n = 11$), 600 μM Fluo-4FF ($n = 7$) and 600 μM Fluo-4FF in Mg^{2+}-free internal solution ($n = 8$). D_{app} for Ca^{2+} in each condition is given by the slope of the linear fit (solid lines). (**d**) Top, fluorescence collected in line scans after photoactivation of NPE-HPTS with brief (0.5 ms) 715-nm laser pulses. Bottom, profile of $\Delta G/R_{HPTS}$ along the dendrite (noisy, thin traces) measured at various times after stimulation. Smooth lines are Gaussian fits. (**e**) As in **d**, for cells loaded with DMNB-FIDx and photoactivated using longer (2 ms) 715-nm laser pulses. (**f**) Estimation of diffusion coefficients within dendrites for HPTS ($n = 16$) and FIDx ($n = 11$). Black arrowhead, time of stimulation.

(CTZ, 50 μM), which reduces the desensitization of AMPARs and prolongs their opening, increased $\Delta G/R_{syn}$ and the EPSC to 151 ± 29% and 139.6 ± 13.8%, respectively, of control levels. Ca^{2+} release from intracellular stores makes a small contribution to $\Delta[Ca]_{syn}$, as CPA reduced $\Delta G/R_{syn}$ to 72.1 ± 4.7% of control levels without affecting the EPSC (101.7 ± 18.7% of control) (**Fig. 5d,e**). CPA did not affect the decay kinetics ($\tau_{\Delta G/R} = 392 \pm 42$ ms) or the spread of $\Delta G/R_{syn}$ ($\sigma_{peak} = 0.63 \pm 0.05$ and $\sigma_{max} = 1.2 \pm 0.14$), indicating that Ca^{2+} sequestration into internal stores does not have a major role in shaping or clearing $\Delta[Ca]_{syn}$ (**Fig. 5f**). Therefore, SCLTD induction and $\Delta[Ca]_{syn}$ share a common requirement for CP-AMPAR activation, consistent with $\Delta[Ca]_{syn}$ being the relevant Ca^{2+} signal for plasticity induction.

Parvalbumin slows the spread of synaptic Ca^{2+} signals

The diffusion of Ca^{2+} in the dendrite may be retarded by interactions with Ca^{2+}-binding proteins (CBPs). The spread of Ca^{2+} may also be limited by physical features of the dendrite, such as cellular organelles, membrane invaginations or molecular crowding, that are not specific to Ca^{2+}. One can distinguish between these possibilities by examining the dependence of the spread of $\Delta G/R_{syn}$ on the concentration and affinity of the Ca^{2+} indicator[31,32]. If low-mobility CBPs prevent the spread of Ca^{2+}, the addition of a large amount of mobile Ca^{2+} indicator will bypass this diffusion barrier and accelerate the spread of Ca^{2+}. In contrast, the effects of physical barriers on the spread of Ca^{2+} are independent of the concentration and affinity of the Ca^{2+} indicator.

We quantified the retardation of Ca^{2+} diffusion in the dendrite by measuring the apparent diffusion coefficient (D_{app}) of Ca^{2+} from the slope of the relationship between increases in $\sigma^2/2$ (that is, $\Delta(\sigma^2/2)$) versus time after stimulation (Δt). Using 300 μM of Fluo-5F to monitor $\Delta[Ca]_{syn}$ (**Fig. 4d**), we calculated $D_{app} = 10.1 \pm 1.2$ μm^2 s^{-1}, which is markedly smaller than the reported mobilities of Ca^{2+} and of structurally similar fluorophores in aqueous solutions[33,34]. $\Delta G/R_{syn}$ was also monitored in stellate cells loaded with 300 μM of Fluo-4FF, an indicator with lower Ca^{2+} affinity that is therefore less effective at shunting barriers posed by CBPs (see equation (4) in **Supplementary Methods** online). In this condition, σ_{peak}, σ_{max} and D_{app} were reduced (0.51 ± 0.02, 1.33 ± 0.08 μm and 5.0 ± 0.8 μm^2 s^{-1}, respectively) compared to the values obtained from cells loaded with 300 μM Fluo-5F (**Fig. 6a**). To confirm that these differences were due to the differential Ca^{2+} binding capacity of the indicators, we repeated these measurements in the presence of 600 μM Fluo-4FF, which is expected to increase σ_{peak}, σ_{max} and D_{app}. In this condition, we measured $\sigma_{peak} = 0.57 \pm 0.05$ μm, $\sigma_{max} = 1.57 \pm 0.07$ μm and $D_{app} = 6.9 \pm 0.5$ μm^2 s^{-1}, values in between those obtained with 300 μM Fluo-4FF and 300 μM Fluo-5F.

Stellate cells express parvalbumin, which binds either Ca^{2+} or magnesium (Mg^{2+}) at a single site[35]. As a result of competitive binding, the apparent affinity for Ca^{2+} increases as $[Mg^{2+}]$ is reduced (apparent

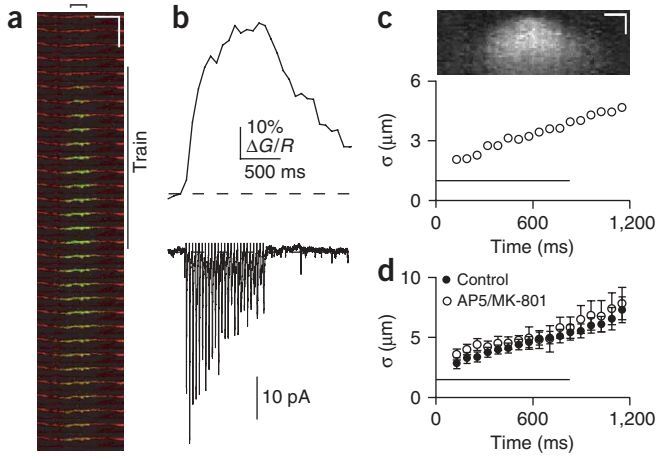

Figure 7 $\Delta[Ca]_{syn}$ remains compartmentalized during sustained synaptic activity. (**a**) Overlaid green and red images of a stellate cell dendrite filled with Alexa-594 and Fluo-4FF collected every 64 ms during trains of activity (average of 5 trials). Vertical line marks the duration of the stimulus train. Scale bars, 5 μm and 150 ms. (**b**) Top, $\Delta G/R_{syn}$ measured in the bracketed region from **a**. Bottom, corresponding EPSCs. (**c**) Top, time-dependent profile of $\Delta G/R_{syn}$ along the dendrite shown in **a**. Bottom, σ of Gaussian fits to the data plotted as a function of time. Scale bars, 2 μm and 600 ms. (**d**) Summary data as in **c** in control (closed circles, $n = 11$) and in the presence of AP5 alone or AP5 and MK-801 (open circles, $n = 6$). Horizontal lines in **c** and **d** indicate the duration of the stimulus train.

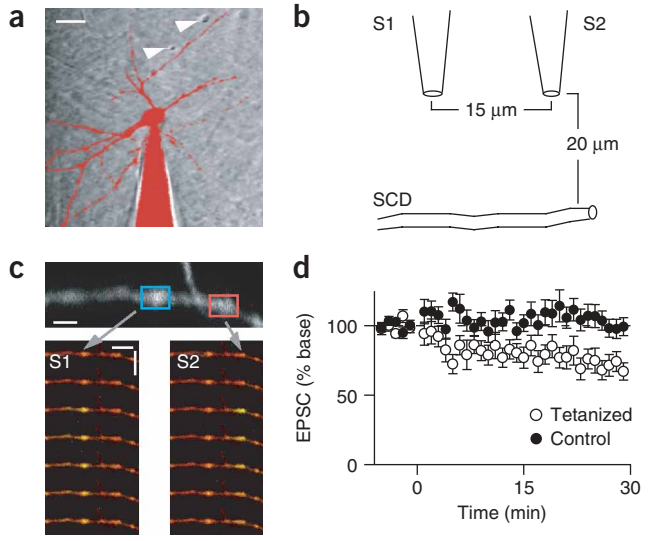

Figure 8 The input specificity of LTD is maintained over short distances. (**a**) Image of a stellate cell filled with Alexa-594 overlaid on an LSDIC image of the slice. Arrowheads, positions of two stimulating electrodes located in the molecular layer. Scale bar, 10 μm. (**b**) Schematic depicting the arrangement of the dendrite and stimulating electrodes (not drawn to scale). (**c**) Top, enlarged image of a stellate cell dendrite filled with Alexa-594 and Fluo-5F. Scale bar, 2 μm. Bottom, overlaid green and red images showing independent $\Delta[Ca]_{syn}$ in response to electrical stimulation through either stimulating electrode S1 or S2. Scale bars, 5 μm and 50 ms. Frames were collected every 64 ms. (**d**) EPSC amplitude in the tetanized and control pathways during SCLTD induction using the stimulus electrode arrangement shown in **a**–**c**.

dissociation constant, K_d, for Ca^{2+} is ~4–9 nM in 0 nM of free Mg^{2+} and ~50 nM in 0.16 mM of free Mg^{2+})[36,37]. In 0 Mg^{2+}, parvalbumin should be saturated by $[Ca^{2+}]$ in an inactive neuron and its ability to buffer further increases in Ca^{2+} will be greatly reduced. If parvalbumin is the dominant CBP that restricts Ca^{2+} diffusion, we predict that the spread of Ca^{2+} should be increased in the absence of intracellular Mg^{2+}. Indeed, using a Mg^{2+}-free internal solution and 600 μM Fluo-4FF, σ_{peak} and σ_{max} increased to 1.13 ± 0.1 and 3.1 ± 0.19 μm, respectively, and D_{app} to 24.5 ± 2.3 $\mu m^2\ s^{-1}$, a threefold increase compared to that in the presence of normal Mg^{2+} (**Fig. 6b**,**c**). Thus, Ca^{2+} binding to parvalbumin normally slows the diffusion of Ca^{2+} in the dendrite. The values of D_{app} obtained in this section were used to derive an analytic model of Ca^{2+} in stellate cell dendrites (**Supplementary Methods** and **Supplementary Fig. 5** online).

General slowing of diffusion in dendrites

As the concentration of a single, dominant Ca^{2+} buffer is increased, D_{app} of Ca^{2+} should approach the diffusion coefficient of the buffer (see equation (4) in **Supplementary Methods**). However, D_{app} measured in the presence of a high concentration of Fluo-4FF and 0 Mg^{2+} was low compared to previously reported values for the diffusion of structurally similar Ca^{2+} indicators[29,34]. This discrepancy either reflects a failure to overwhelm the Ca^{2+}-binding capacity of CBPs or indicates the existence of additional mechanisms that slow the diffusion of the Ca^{2+} indicator. To determine if stellate cell dendrites generally retard small molecule diffusion, we monitored the movement of photoactivatable, Ca^{2+}-insensitive fluorophores. We used combined 2PLSM and two-photon laser uncaging (2PLU)[38,39] to measure the spread of a 524-Da fluorophore, 8-hydroxypyrene-1,3,6-trisulfonic acid (HPTS), following photolysis of its nonfluorescent caged version, *o*-1(2-nitrophenyl)ethyl ether cage (NPE-HPTS)[40]. Brief (0.5 ms) laser pulses at 715 nm caused an increase in green fluorescence ($\Delta G/R_{HPTS}$), corresponding to photorelease of HPTS (**Fig. 6d**). The diffusion coefficient of HPTS within stellate cell dendrites (D_{HPTS}) was ~24.1 ± 3.3 $\mu m^2\ s^{-1}$, approximately 10% of the value in aqueous solutions[41]. As HPTS may interact with cellular proteins through its negative charge, we also measured the mobility of anionic fluorescent dextrans. 2PLU of 2,3-dimethyl-2,3-dinitrobutane fluorescein-conjugated dextran (DMNB-FlDx, 1 mM) yielded D_{FlDx} ~ 11.4 ± 1.7 $\mu m^2\ s^{-1}$, which is also approximately 10% of the value in aqueous environments[42] (**Fig. 6e**,**f**). Thus, stellate cell dendrites retard diffusional equilibration by means of a general barrier to the movement of small molecules.

Ca^{2+} compartmentalization during repetitive stimulation

Are stellate cell dendrites able to compartmentalize Ca^{2+} during sustained synaptic activation that induces input-specific synaptic plasticity? To address this question, we loaded stellate cells with 300 μM Fluo-4FF and measured $\Delta G/R_{syn}$ during trains of 25 stimuli delivered to parallel fibers at 30 Hz (**Fig. 7**). To minimize photodamage during prolonged imaging, $\Delta G/R_{syn}$ was measured in frame-scan mode at 15.6 Hz and the profile of $\Delta G/R_{syn}$ along the dendrite was calculated for each frame (**Fig. 7a**–**c**). Train-evoked $\Delta[Ca]_{syn}$ was restricted to small dendritic segments (σ_{peak} = 5.4 ± 0.46 μm and σ_{max} = 7.3 ± 0.8 μm), indicating Ca^{2+} compartmentalization during moderate frequency stimulation (**Fig. 7d**). The greater spread of Ca^{2+} along the dendrite after trains compared to that found with single stimuli probably reflects the greater time for diffusion between the start of stimulation and the measurement of σ_{peak} in each experiment (~120 ms versus ~10 ms). In addition, the spread of Ca^{2+} was increased by the effects of Ca^{2+} indicators (**Supplementary Fig. 5** and **Supplementary Methods**). Sustained activity may also recruit extrasynaptic NMDARs, which broaden the region over which Ca^{2+} enters the dendrite. However, in the presence of NMDAR antagonists (100 μM AP5 and 50 μM MK-801), the spread of $\Delta G/R_{syn}$ was the same as in the control conditions (σ_{peak} = 5.8 ± 0.63, σ_{max} = 7.8 ± 0.95; n = 6) (**Fig. 7d**), suggesting that extrasynaptic NMDARs do not substantially contribute to $\Delta[Ca]_{syn}$ during repeated synaptic activity at resting potentials.

Closely-spaced synapses are independently regulated

Our data indicate that synaptically evoked Ca^{2+} signals are restricted to small dendritic stretches surrounding the active synapses, suggesting that even closely spaced synapses on the same dendritic branch can be modulated independently. To test this hypothesis, we filled stellate cells with Alexa-594 and Fluo-5F and identified an arrangement of stimulating electrodes that activated neighboring sets of synapses (**Fig. 8**). Two stimulating electrodes were placed 10–15 μm apart and approximately 20 μm from the dendrite (**Fig. 8a**,**b**). Given the regular spacing and linear course of parallel fibers, we predicted that this arrangement will activate closely spaced groups of synapses on the visualized dendrite. This was confirmed by the visualization of the synaptically evoked Ca^{2+} transients, demonstrating an intersynaptic distance of 10.2 ± 1.3 μm (range 6–13 μm, n = 8) (**Fig. 8c**). In separate experiments, stellate cells were loaded with Alexa-594 but no Ca^{2+} indicator, and the same electrode configuration was used to test the input specificity of SCLTD for these closely spaced synapses. SCLTD of the tetanized pathway was similar to that described above (27.5 ± 2.7%) and retained its input specificity such that the control pathway was unaffected by the induction protocol (102.5 ± 4.2%) (**Fig. 8d**).

DISCUSSION

Here we show that stellate cells independently regulate active synapses by a Ca^{2+}- and endocannabinoid-dependent form of LTD (SCLTD). As the expression of SCLTD is limited to the synapses that experienced the induction protocol, stellate cell dendrites compartmentalize not only the postsynaptic Ca^{2+} signals, but also the downstream signaling cascades that lead to the production of endocannabinoids. We demonstrated that stellate cell dendrites are endowed with specializations that create spatially isolated Ca^{2+} signaling domains after single and sustained synaptic stimulation. These specializations include diffusion barriers that are specific to Ca^{2+}, such as low-mobility Ca^{2+}-binding proteins, as well as general barriers to small molecule diffusion.

Induction and expression of SCLTD

The long-term plasticity of parallel fiber–to–stellate cell synapses has been described previously[11,12]. In the best-characterized form of plasticity, prolonged activity (300 stimuli at 50 Hz) triggers the replacement of CP-AMPARs by CI-AMPARs (ref. 11). Because CP-AMPARs have higher overall permeability than CI-AMPARs, this switch results in a depression of synaptic currents at resting potentials. However, due to the inward rectification of CP-AMPARs in the presence of intracellular polyamines, this switch increases synaptic current measured at positive potentials. In contrast, we found that SCLTD reduces the amplitude of synaptically evoked currents at both positive and negative potentials and does not affect EPSC rectification. SCLTD induction increases the coefficient of variability of the EPSC, the failure rate of synaptic transmission, and paired-pulse facilitation. These changes are consistent with the decreased probability of glutamate release from presynaptic terminals, as is expected from the known actions of endocannabinoids on parallel fiber boutons[20,21,23,24,43]. We found that SCLTD requires the activation of CP-AMPARs, mGluR1s and CB1Rs, and an increase in postsynaptic $[Ca^{2+}]$. SCLTD does not require Ca^{2+} release from internal stores, suggesting that mGluR1 activation and Ca^{2+} buildup due to CP-AMPAR opening interact to facilitate endocannabinoid production, as has been described at the parallel fiber–to–Purkinje cell synapse[23,44].

Mechanisms of compartmentalization in stellate cells

Synaptically localized CP-AMPARs provide a focal source of Ca^{2+} and their activation will necessarily produce a spatially nonhomogeneous Ca^{2+} signal in the dendrite. Thus the relevant analysis is whether dendrites possess specializations that prevent the spread of Ca^{2+} after its entry into the dendrite. In aspiny dendrites of cortical fast-spiking interneurons, brief activation of synaptic Ca^{2+} sources and rapid clearance of Ca^{2+} from the cytoplasm in perisynaptic areas are thought to create postsynaptic Ca^{2+} signaling compartments[9]. In stellate cells, the long-lived gradients in dendritic $[Ca^{2+}]$ seen after synaptic stimulation result from specializations that slow the diffusion of Ca^{2+} and other molecules away from synaptic sites. Notably, the apparent diffusion coefficient of Ca^{2+} (D_{app}) in stellate cell dendrites is only 4–11 $\mu m^2\ s^{-1}$, depending on the concentration and affinity of the indicator used to monitor Ca^{2+}. This represents nearly 100-fold retardation relative to the mobility of Ca^{2+} in aqueous solutions ($\sim$700 $\mu m^2\ s^{-1}$) and in the cytoplasm of various cell types ($\sim$200–400 $\mu m^2\ s^{-1}$)[45].

The pronounced slowing of Ca^{2+} diffusion results from two mechanisms. First, a general barrier to diffusion impedes the movement of all molecules within the stellate cell dendrites. The mobility of HPTS and fluorescein-conjugated dextrans indicates diffusion coefficients of $\sim$24 $\mu m^2\ s^{-1}$ and $\sim$11 $\mu m^2\ s^{-1}$, respectively, in stellate cell dendrites. These values are markedly smaller than those reported for the same molecules in aqueous solutions[41,42] and for similar molecules in the cytosol of multiple preparations[33,41,45–47], revealing a general barrier to diffusion. Such a barrier might result from the high viscosity, molecular crowding or tortuosity of the dendroplasm[33,47,48] and is expected to retard the movement of all molecules, including second messengers (such as Ca^{2+} and cAMP) and proteins (such as kinases, phosphatases and CBPs). Second, the mobility of Ca^{2+} in the dendrite is further restricted by interactions with parvalbumin, a CBP that is highly expressed in stellate cells. Reducing the sensitivity of Ca^{2+} mobility to parvalbumin by lowering intracellular Mg^{2+} increased D_{app} to $\sim$25 $\mu m^2\ s^{-1}$, the same diffusion coefficient measured for HPTS ($\sim$24 $\mu m^2\ s^{-1}$). Given the similar molecular weight, charge and aromatic structure of HPTS and Fluo-4FF, this value probably represents the upper limit of diffusion for such molecules in the dendrite.

Ca^{2+} compartmentalization in unperturbed stellate cells

The spatiotemporal profile of synaptically evoked Ca^{2+} transients measured in stellate cell dendrites was broadened (**Fig. 6**) and prolonged (**Supplementary Fig. 5**) when the buffering capacity of the Ca^{2+} indicator was increased. A theoretical framework exists for quantifying these effects of the indicator on Ca^{2+} transients[31]. Using this framework and the data presented in **Figures 6** and **7**, we formulated an analytical model of Ca^{2+} diffusion in the dendrite (**Supplementary Methods**) that reproduces the measured spatiotemporal profiles of Ca^{2+} produced by single and repetitive synaptic stimulation (**Supplementary Fig. 5**). By setting the concentration of added Ca^{2+} indicator to 0, we used the model to estimate the spread of Ca^{2+} from the synapse in unperturbed neurons[31]. We found that, in the absence of exogenous buffers, synaptically evoked Ca^{2+} transients were confined to a segment of dendrite approximately 1 µm in length, such that at a distance of 500 nm from the Ca^{2+} source, $[Ca^{2+}]$ reaches only 14% of the peak value reached at the source. Similarly, during repetitive stimulation of the synapse as used in the induction of SCLTD, Ca^{2+} is confined to a roughly 2-µm length of dendrite around the active synapse, such that the peak reached 1 µm from the Ca^{2+} source is only 22% of the peak at the source. This tight compartmentalization of Ca^{2+} during prolonged stimulation is necessary for the independent regulation of closely spaced synapses located on a single dendrite (**Fig. 8**).

Summary

We conclude that, despite the absence of dendritic spines, stellate cell dendrites compartmentalize multistep signaling cascades such as that leading from AMPAR opening to CB1 receptor activation. This cascade involves at least two diffusible second messengers—Ca^{2+} and endocannabinoids—yet synapses located only $\sim$10 µm from each other can be independently regulated. As required for this specificity, synaptically evoked dendritic Ca^{2+} transients are confined to small stretches surrounding active synapses. Furthermore, through the quantitative analysis of the effects of Ca^{2+} indicators on evoked Ca^{2+} transients, we showed that in unperturbed stellate cells, synaptically evoked Ca^{2+} transients are confined to perisynaptic dendritic stretches $\sim$1 µm and 2 µm in length during single and sustained stimulation, respectively.

METHODS

Slice preparation. Sprague-Dawley rats (postnatal day 15–20) were decapitated after deep isoflurane anesthesia. The cerebellum was removed and placed in ice-cold dissection media consisting of 110 mM choline chloride, 25 mM sodium bicarbonate, 11.6 mM sodium ascorbate, 7.0 mM $MgCl_2$, 3.1 mM pyruvic acid, 1.25 mM sodium phosphate, 2.5 mM KCl, 0.5 mM $CaCl_2$ and 25 mM glucose. Transverse (majority of plasticity experiments) or sagittal (majority of imaging experiments) slices were cut in 300-µm-thick sections using a vibratome (Leica,

VT1000S) and transferred to an incubation chamber containing artificial cerebrospinal fluid (ACSF) consisting of 127 mM NaCl, 25 mM sodium bicarbonate 3 mM $CaCl_2$, 2.5 mM KCl, 1.25 mM sodium phosphate, 1 mM $MgCl_2$ and 25 mM glucose. Slices were incubated for 30–45 min at 34 °C and then kept at room temperature until use. All animal handling was performed in accordance with Harvard and federal guidelines.

Whole-cell recordings. Slices were transferred to a submerged recording chamber perfused with room-temperature (22–25 °C) ACSF. Bicuculline (20 μM) was added to block $GABA_A$ receptors. The following drugs were applied either in the bath or with local perfusion using a picospritzer (Parker Instrumentation): 20 μM or 100 μM AP5, 50 μM MK-801, 10 μM NBQX, 10 μM or 50 μM NHPP-spermine, 50 μM CTZ, 50 μM CPA, 2 μM AM-251 and 50 μM CPCCOEt. Stellate cells in the outer third of the molecular layer were voltage-clamped at –60 mV. Electrodes were filled with 130 mM cesium methanesulfonate, 10 mM HEPES buffer, 10 mM sodium phosphocreatine, 4 mM $MgCl_2$, 4 mM Na-ATP, 0.4 mM Na-GTP, 1 mM QX-314 and 0.2 mM EGTA. We included 0.1 mM spermine for rectification measurements. EPSCs were evoked by small, brief (50–200 μA, 0.2 ms) current injections delivered to parallel fibers via glass pipettes. For Ca^{2+} imaging, EGTA was replaced with 300 μM Fluo-5F ($K_d \sim 1.6$ μM) or with 300 μM or 600 μM Fluo4-FF ($K_d \sim 10.4$ μM) and 20 μM Alexa Fluor-594 (refs. 26,49). Experiments involving plasticity over close distances (see below) were performed with an intracellular solution containing EGTA and Alexa Fluor-594. To monitor photorelease of caged fluorophores, cells were loaded with 5 μM Alexa-594 and 1 mM of DMNB-fluorescein conjugated to a 3-kDa dextran (FlDx) or NPE-HPTS (ref. 40). NPE-HPTS was provided by J.E.T. Corrie and D. Ogden (National Institute for Medical Research, London). All other fluorophores were obtained from Molecular Probes.

Long-term plasticity. Two stimulating electrodes separated by 30–40 μm were positioned 80–100 μm from the cell body. We verified the independence of the pathways by ensuring that stimulation of one pathway did not produce paired-pulse facilitation in the other pathway. A stimulus was delivered every 5 s to each pathway in turn, in order to monitor basal responses to each set of inputs. Baseline responses were recorded for 5 min. One pathway was tetanized with 4 trains of 25 stimuli at 30 Hz delivered at 0.33 Hz. Stimulation as in the baseline period was resumed to monitor the effect of the stimulus trains on each pathway. For experiments in which the effects of NHPP-spermine or CPA were tested, slices were incubated in the presence of the drug for at least 45 min before use. As a positive control for the actions of CPA, we examined caffeine-induced Ca^{2+} transients in Purkinje cells and found that CPA abolished evoked transients within 4 min of application (**Supplementary Fig. 1**). PPF was measured as the response to pairs of pulses (15 ms interpulse interval) delivered every 20 s in a single pathway; PPF was defined as P2/P1 − 1, where *P*2 and *P*1 are the amplitudes of the second and first EPSC, respectively.

EPSC amplitude during the baseline period was 83–399 pA in the control pathway (mean ± s.e.m.: 211.6 ± 26.8) and 90–385 pA in the tetanized pathway (168.1 ± 17.6) ($P = 0.19$). The reported miniature EPSC amplitude in stellate cells is ~80 pA (refs. 22,27), similar to the mean amplitude of 98.4 ± 16.8 pA that we observed during stimulation of single synapses (**Fig. 3**). Therefore, the EPSC in the baseline period arose from the simultaneous activation of ~1–5 synapses.

For the experiments shown in **Figure 8**, we used fluorescence and laser-scanning differential interference contrast (LSDIC) to position electrodes ~20 μm above spatially isolated dendrites and ~15 μm apart from each other. We determined the stimulus intensity needed to evoke EPSCs of approximately 200 pA in one of the pathways; this intensity was used during the LTD induction tetanus.

All experiments included in the analysis met the following criteria: (i) the induction protocol was delivered no later than 15 min after the recordings commenced; (ii) series resistance was stable to within 20% of the average value during the baseline period; and (iii) at least 25 min of recording were obtained after the induction protocol.

Two-photon microscopy and uncaging. We monitored dendritic fluorescence transients and achieved two-photon laser photoactivation as described previously[38,39]. For $\Delta[Ca]_{syn}$ measurements, the imaging laser was tuned to 810 nm. For simultaneous 2PLSM and 2PLU, the imaging laser was tuned to 810 nm (DMNB-FlDx) or 850 nm (NPE-HPTS), and the photoactivating laser was tuned to 715 nm.

Data acquisition and analysis. EPSCs were recorded in whole-cell voltage-clamp (Multiclamp 700A, Axon Instruments), filtered at 2 kHz and digitized at 10 kHz. Series resistance and whole-cell capacitance were not compensated. Time 0 was defined as the time at which the induction protocol began. To calculate percent LTD, the average EPSC amplitude during minutes 25–30 after induction was compared to the average EPSC amplitude during the baseline period. To quantify changes in rectification, we recorded current-voltage (*I-V*) relationships at holding potentials between –60 mV and +60 mV and made linear fits to the *I-V* plots in the range of –60 mV to –20 mV. The junction potential of 9 mV was corrected for these measurements. The RI was defined as the ratio of the measured current at +60 mV to the linearly predicted value at +60 mV (ref. 11).

We performed image acquisition using ScanImage[50]. Green and red fluorescence were acquired simultaneously during 500-Hz line scans along dendritic shafts or during 15.6-Hz frame scans. Fluorescence changes were quantified as increases in green fluorescence divided by red fluorescence ($\Delta G/R$) (ref. 26). We measured $\Delta G/R$ at saturation ($\Delta G/R_{max}$) for Fluo-5F and Fluo-4FF (0.9 and 1.2, respectively, with 300 μM indicator dye and 20 μM AF-594) and at rest ($\Delta G/R_{rest}$; <0.1). During single stimulus experiments, $\Delta G/R$ signals (<0.15) were <20% of $\Delta G/R_{max} - \Delta G/R_{rest}$, giving a linearity error of <20%. During train experiments, $\Delta G/R$ signals were <0.4, with linearity errors of <36%.

To estimate diffusion coefficients within stellate cell dendrites, $\Delta G/R$ was calculated as a function of space along the dendrite and fit with Gaussian functions. The standard deviation of the Gaussian, $\sigma(t)$, is related to the diffusion coefficient D of the fluorescent molecule by $D = (1/2) \cdot d[\sigma^2(t)]/dt$. Thus, D is given by the slope of a plot of $\sigma^2/2$ versus time. For measurements of Ca^{2+} spread during extended stimulus trains, we acquired two-dimensional images at 15.6 Hz. These were collapsed in the direction transverse to the orientation of the dendrite to produce a one-dimensional fluorescence profile, which was carried through the same analysis described above. Data is presented as mean ± s.e.m. For statistical comparisons, we used the two-tailed Student's *t*-test. Differences were considered significant if $P < 0.05$.

Note: Supplementary information is available on the Nature Neuroscience website.

ACKNOWLEDGMENTS

We thank members of the Sabatini lab and W. Regehr for helpful discussions, and J. Corrie and D. Ogden for the gift of NPE-HPTS. This work was funded by the National Institutes of Neurological Disorders and Stroke (1 F31 NS049655-01) and Quan predoctoral fellowships to G.J.S.L., and a Burroughs Wellcome Fund Career Award, a Searle Scholar award, and McKnight Foundation Technological Innovations Awards to B.L.S.

COMPETING INTERESTS STATEMENT

The authors declare that they have no competing financial interests.

Published online at http://www.nature.com/natureneuroscience
Reprints and permissions information is available online at http://npg.nature.com/reprintsandpermissions/

1. Nimchinsky, E.A., Sabatini, B.L. & Svoboda, K. Structure and function of dendritic spines. *Annu. Rev. Physiol.* **64**, 313–353 (2002).
2. Palay, S.L. & Chan-Palay, V. *The Stellate Cell*, 216–233 (Strange-Verlag, New York, 1974).
3. Freund, T.F. & Buzsaki, G. Interneurons of the hippocampus. *Hippocampus* **6**, 347–470 (1996).
4. McMahon, L.L. & Kauer, J.A. Hippocampal interneurons express a novel form of synaptic plasticity. *Neuron* **18**, 295–305 (1997).
5. Cowan, A.I., Stricker, C., Reece, L.J. & Redman, S.J. Long-term plasticity at excitatory synapses on aspinous interneurons in area CA1 lacks synaptic specificity. *J. Neurophysiol.* **79**, 13–20 (1998).
6. Rozsa, B., Zelles, T., Vizi, E.S. & Lendvai, B. Distance-dependent scaling of calcium transients evoked by backpropagating spikes and synaptic activity in dendrites of hippocampal interneurons. *J. Neurosci.* **24**, 661–670 (2004).
7. Kaiser, K.M., Lubke, J., Zilberter, Y. & Sakmann, B. Postsynaptic calcium influx at single synaptic contacts between pyramidal neurons and bitufted interneurons in layer 2/3 of rat neocortex is enhanced by backpropagating action potentials. *J. Neurosci.* **24**, 1319–1329 (2004).

8. Topolnik, L., Congar, P. & Lacaille, J.C. Differential regulation of metabotropic glutamate receptor- and AMPA receptor-mediated dendritic Ca^{2+} signals by presynaptic and postsynaptic activity in hippocampal interneurons. *J. Neurosci.* **25**, 990–1001 (2005).
9. Goldberg, J.H., Tamas, G., Aronov, D. & Yuste, R. Calcium microdomains in aspiny dendrites. *Neuron* **40**, 807–821 (2003).
10. Hausser, M. & Clark, B.A. Tonic synaptic inhibition modulates neuronal output pattern and spatiotemporal synaptic integration. *Neuron* **19**, 665–678 (1997).
11. Liu, S.Q. & Cull-Candy, S.G. Synaptic activity at calcium-permeable AMPA receptors induces a switch in receptor subtype. *Nature* **405**, 454–458 (2000).
12. Rancillac, A. & Crepel, F. Synapses between parallel fibres and stellate cells express long-term changes in synaptic efficacy in rat cerebellum. *J. Physiol. (Lond.)* **554**, 707–720 (2004).
13. Kosaka, T., Kosaka, K., Nakayama, T., Hunziker, W. & Heizmann, C.W. Axons and axon terminals of cerebellar Purkinje cells and basket cells have higher levels of parvalbumin immunoreactivity than somata and dendrites: quantitative analysis by immunogold labeling. *Exp. Brain Res.* **93**, 483–491 (1993).
14. Bowie, D. & Mayer, M.L. Inward rectification of both AMPA and kainate subtype glutamate receptors generated by polyamine-mediated ion channel block. *Neuron* **15**, 453–462 (1995).
15. Kamboj, S.K., Swanson, G.T. & Cull-Candy, S.G. Intracellular spermine confers rectification on rat calcium-permeable AMPA and kainate receptors. *J. Physiol. (Lond.)* **486**, 297–303 (1995).
16. Koh, D.S., Burnashev, N. & Jonas, P. Block of native Ca(2+)-permeable AMPA receptors in rat brain by intracellular polyamines generates double rectification. *J. Physiol. (Lond.)* **486**, 305–312 (1995).
17. Carter, A.G. & Regehr, W.G. Prolonged synaptic currents and glutamate spillover at the parallel fiber to stellate cell synapse. *J. Neurosci.* **20**, 4423–4434 (2000).
18. Washburn, M.S. & Dingledine, R. Block of alpha-amino-3-hydroxy-5-methyl-4-isoxazolepropionic acid (AMPA) receptors by polyamines and polyamine toxins. *J. Pharmacol. Exp. Ther.* **278**, 669–678 (1996).
19. Herkenham, M. Cannabinoid receptor localization in brain: relationship to motor and reward systems. *Ann. NY Acad. Sci.* **654**, 19–32 (1992).
20. Kreitzer, A.C. & Regehr, W.G. Retrograde inhibition of presynaptic calcium influx by endogenous cannabinoids at excitatory synapses onto Purkinje cells. *Neuron* **29**, 717–727 (2001).
21. Maejima, T., Ohno-Shosaku, T. & Kano, M. Endogenous cannabinoid as a retrograde messenger from depolarized postsynaptic neurons to presynaptic terminals. *Neurosci. Res.* **40**, 205–210 (2001).
22. Rancillac, A. & Barbara, J.G. Frequency-dependent recruitment of inhibition mediated by stellate cells in the rat cerebellar cortex. *J. Neurosci. Res.* **80**, 414–423 (2005).
23. Brown, S.P., Brenowitz, S.D. & Regehr, W.G. Brief presynaptic bursts evoke synapse-specific retrograde inhibition mediated by endogenous cannabinoids. *Nat. Neurosci.* **6**, 1048–1057 (2003).
24. Brenowitz, S.D. & Regehr, W.G. Calcium dependence of retrograde inhibition by endocannabinoids at synapses onto Purkinje cells. *J. Neurosci.* **23**, 6373–6384 (2003).
25. Safo, P.K. & Regehr, W.G. Endocannabinoids control the induction of cerebellar LTD. *Neuron* **48**, 647–659 (2005).
26. Sabatini, B.L., Oertner, T.G. & Svoboda, K. The life cycle of Ca^{2+} ions in dendritic spines. *Neuron* **33**, 439–452 (2002).
27. Carter, A.G. & Regehr, W.G. Quantal events shape cerebellar interneuron firing. *Nat. Neurosci.* **5**, 1309–1318 (2002).
28. Zador, A. & Koch, C. Linearized models of calcium dynamics: formal equivalence to the cable equation. *J. Neurosci.* **14**, 4705–4715 (1994).
29. Gabso, M., Neher, E. & Spira, M.E. Low mobility of the Ca^{2+} buffers in axons of cultured Aplysia neurons. *Neuron* **18**, 473–481 (1997).
30. Toth, K. & McBain, C.J. Afferent-specific innervation of two distinct AMPA receptor subtypes on single hippocampal interneurons. *Nat. Neurosci.* **1**, 572–578 (1998).
31. Neher, E. & Augustine, G.J. Calcium gradients and buffers in bovine chromaffin cells. *J. Physiol. (Lond.)* **450**, 273–301 (1992).
32. Zhou, Z. & Neher, E. Mobile and immobile calcium buffers in bovine adrenal chromaffin cells. *J. Physiol. (Lond.)* **469**, 245–273 (1993).
33. Kushmerick, M.J. & Podolsky, R.J. Ionic mobility in muscle cells. *Science* **166**, 1297–1298 (1969).
34. Michailova, A., DelPrincipe, F., Egger, M. & Niggli, E. Spatiotemporal features of Ca^{2+} buffering and diffusion in atrial cardiac myocytes with inhibited sarcoplasmic reticulum. *Biophys. J.* **83**, 3134–3151 (2002).
35. Hou, T.T., Johnson, J.D. & Rall, J.A. Parvalbumin content and Ca^{2+} and Mg^{2+} dissociation rates correlated with changes in relaxation rate of frog muscle fibres. *J. Physiol. (Lond.)* **441**, 285–304 (1991).
36. Lee, S.H., Schwaller, B. & Neher, E. Kinetics of Ca^{2+} binding to parvalbumin in bovine chromaffin cells: implications for $[Ca^{2+}]$ transients of neuronal dendrites. *J. Physiol. (Lond.)* **525**, 419–432 (2000).
37. Li-Smerin, Y., Levitan, E.S. & Johnson, J.W. Free intracellular Mg^{2+} concentration and inhibition of NMDA responses in cultured rat neurons. *J. Physiol. (Lond.)* **533**, 729–743 (2001).
38. Carter, A.G. & Sabatini, B.L. State-dependent calcium signaling in dendritic spines of striatal medium spiny neurons. *Neuron* **44**, 483–493 (2004).
39. Bloodgood, B.L. & Sabatini, B.L. Neuronal activity regulates diffusion across the neck of dendritic spines. *Science* **310**, 866–869 (2005).
40. Jasuja, R., Keyoung, J., Reid, G.P., Trentham, D.R. & Khan, S. Chemotactic responses of *Escherichia coli* to small jumps of photoreleased L-aspartate. *Biophys. J.* **76**, 1706–1719 (1999).
41. Xia, P., Bungay, P.M., Gibson, C.C., Kovbasnjuk, O.N. & Spring, K.R. Diffusion coefficients in the lateral intercellular spaces of Madin-Darby canine kidney cell epithelium determined with caged compounds. *Biophys. J.* **74**, 3302–3312 (1998).
42. Svoboda, K., Tank, D.W. & Denk, W. Direct measurement of coupling between dendritic spines and shafts. *Science* **272**, 716–719 (1996).
43. Levenes, C., Daniel, H., Soubrie, P. & Crepel, F. Cannabinoids decrease excitatory synaptic transmission and impair long-term depression in rat cerebellar Purkinje cells. *J. Physiol. (Lond.)* **510**, 867–879 (1998).
44. Maejima, T. *et al.* Synaptically driven endocannabinoid release requires Ca^{2+}-assisted metabotropic glutamate receptor subtype 1 to phospholipase Cbeta4 signaling cascade in the cerebellum. *J. Neurosci.* **25**, 6826–6835 (2005).
45. Allbritton, N.L., Meyer, T. & Stryer, L. Range of messenger action of calcium ion and inositol 1,4,5-trisphosphate. *Science* **258**, 1812–1815 (1992).
46. Strautman, A.F., Cork, R.J. & Robinson, K.R. The distribution of free calcium in transected spinal axons and its modulation by applied electrical fields. *J. Neurosci.* **10**, 3564–3575 (1990).
47. Popov, S. & Poo, M.M. Diffusional transport of macromolecules in developing nerve processes. *J. Neurosci.* **12**, 77–85 (1992).
48. Ellis, R.J. Macromolecular crowding: obvious but underappreciated. *Trends Biochem. Sci.* **26**, 597–604 (2001).
49. Yasuda, R. *et al.* Imaging calcium concentration dynamics in small neuronal compartments. *Sci. STKE* **2004**, pl5 (2004).
50. Pologruto, T.A., Sabatini, B.L. & Svoboda, K. ScanImage: flexible software for operating laser scanning microscopes. *Biomed. Eng. Online* **2**, 13 (2003).